Efficient Intensity Measures of Slide-Rocking Structures for Precariously Balanced Rocks

Taylor J. Knickerbocker[1], Christine E. Wittich[2]

[1] M.S. Student, Department of Civil Engineering, University of Nebraska-Lincoln, Lincoln, NE, USA.
[2] Assistant Professor, Department of Civil Engineering, University Nebraska-Lincoln, Lincoln, NE, USA.

ABSTRACT

Precariously balanced rocks (PBRs) and other fragile geologic features are important in both the engineering and seismological communities since they are indicative of the maximum ground motion at a site over the rock's lifetime. Precariously balanced rocks are individual or stacks of freestanding rocks that tend to respond in rigid body modes when subject to seismic excitation – namely, rocking, sliding, slide-rocking, and free-flight, which can lead to overturning. The seismic response of freestanding structures, such as PBRs, is known to be extremely sensitive to small changes in geometry, position, and earthquake excitation. As such, deterministic methods are limited in their application to PBRs and reliable probabilistic relationships are necessary. Previous probabilistic studies on freestanding structures and PBRs have focused on a single response mode, such as overturning, and utilized a single intensity measure, typically the peak ground acceleration. To this end, this paper aims to identify optimal ground motion intensity measures (IMs) that correlate well with the multiple possible rigid body modes including rocking and sliding. In this study, structural parameters, including geometry and friction, were varied to induce each of the fundamental rigid body modes. The response of each structure was simulated to 3750 analytical pulse motions through numerical integration of the slide-rocking equations of motion within MATLAB. The results of the simulations were statistically analyzed to determine the optimal IMs in terms of both sufficiency and efficiency. A set of viable IMs are presented that have more robust probabilistic relationships with the dynamic response of a sliding or rocking block compared to previous IM studies.

Keywords: rocking, sliding, freestanding structures, precariously balanced rocks, intensity measure

INTRODUCTION

Precariously balanced rocks (PBRs) have been identified as potential natural seismoscopes for the past few decades since their fragile or precarious configurations limit the intensity of earthquake ground motions experienced at the site [1, 2]. This information is incredibly valuable to engineers and seismologists alike because the ground motion at which a PBR overturns is indicative of an upper bound for seismic design. PBRs are individual or stacks of boulders that have eroded into highly precarious or fragile configurations – see Figure 1a. While PBRs have been documented by seismologists since the early 1800s, Brune proposed that the existence of certain PBRs in southern California implied that current seismic hazard was overestimating earthquakes with long recurrence intervals [1, 3]. Since then, numerous studies have been conducted to analyze whether there is a discrepancy between PBRs and hazard curves produced through probabilistic seismic hazard analysis (PSHA). These findings are dependent on location; however, several PBR analyses have indicated that current seismic hazard is overestimated at long return periods.

The critical pieces of information needed to effectively use PBRs as a way to understand rare seismic hazard are the age of the rocks and the ground motion that would overturn them. Two frequently used dating methods include rock-varnish microlamination and cosmogenic-nuclide exposure dating [4, 5]. The rock-varnish method harnesses the knowledge of the elements that would be present in the varnish by geologic time period; and, the oldest geologic time period identified in the varnish can be used to estimate the minimum age for the PBR [4]. On the other hand, cosmogenic-nuclide dating estimates the maximum age of the PBR by measuring the presence of cosmogenic nuclides on the surface of the PBR, which are a function of exposure to the sun's rays [5]. Although these methods are not able to provide a precise age of an individual PBR, they provide an approximate range of how long a PBR has been in a fragile (exhumed) state. Bell et al. utilized both rock-varnish and cosmogenic dating for PBRs in California and Nevada and found the granitic rocks to range from 10,500 to 27,000 years old [4]. In addition to the approximate age of the PBR, knowledge of the motion required to overturn the PBR is necessary. The seismic response of PBRs is akin to that of freestanding structures, since the PBRs have eroded into unattached boulders. To this end, several studies have utilized the theoretical equations of motion for a two-dimensional rocking response to analyze PBRs [6-9]. However, as a freestanding structure, PBRs will respond in a combination of rigid body modes – namely, rocking, sliding, slide-rocking, or free-flight. Relatively few studies have been conducted that account for the multi-modal behavior of

PBRs [e.g., 2]. While this multi-modal behavior more accurately reflects the behavior of a freestanding structure to a given earthquake, the extension to probabilistic relationships is difficult given the potential for the individual modes to correlate with different measures of earthquake intensity.

This paper aims to identify optimal intensity measures for freestanding structures considering both rocking and sliding modes. To this end, the equations of motion for the individual response modes are derived and presented in the first section. Analytical pulse motions to be used as input excitations are discussed in the second section of this paper. Ultimately, an intensity measure study is presented in which the response of freestanding structures is correlated to various potential measures of earthquake intensity.
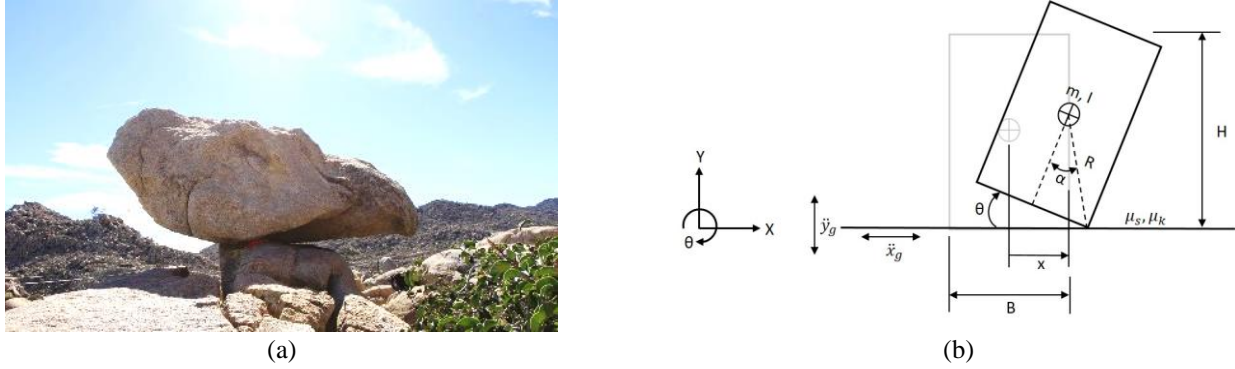

Figure 1. (a) Sample PBR in Jacumba, CA. (b) General sign convention for 2D rigid block.

EQUATIONS OF MOTION

Background

A precariously balanced rock (PBR) can be treated as a freestanding structure, characterized by an unanchored or unattached base and predominantly rigid behavior. These structures respond to earthquakes in some combination of rigid body modes, including rocking, sliding, and slide-rocking. While PBRs are complex, three-dimensional structures, a rectangular two-dimensional block is analyzed herein. The motivation is to reduce uncertainty and to hone in on the fundamental behavior of freestanding structures. A schematic of the general two-dimensional block analyzed is presented in Figure 1b. As shown in this diagram, rotation of the rigid body, θ, is considered positive in the clockwise direction, and horizontal displacement, x, is positive to the right. From Figure 1b, the constants of the rocking block problem are as follows: B is the base length, H is the height, R is the distance from one bottom corner to the centroid, m is the mass, I is the moment of inertia, μ_s is the coefficient of static friction, μ_k is the coefficient of kinetic friction, and α is the critical angle. $\ddot{x}_g$ and $\ddot{y}_g$ represent the horizontal and vertical acceleration components of the input ground motion, respectively. The governing equations of motion for a two-dimensional rigid block subject to horizontal base accelerations have been previously derived and presented by others and are summarized herein [10 – 12].

Sliding

A sliding response is initiated from rest when

$$\mu_s\big(g + \ddot{y}_g\big) < \big|\ddot{x}_g\big| \tag{1}$$

In this equation, the horizontal and vertical ground accelerations are denoted as $\ddot{x}_g$ and $\ddot{y}_g$. Other variables in Eq. (1) include the acceleration due to gravity (g) and the coefficient of static friction (μ_s). This paper's sign convention indicates that horizontal displacement towards the right is positive and displacement towards the left is negative. The equation of motion for a sliding block is:

$$\ddot{x} = -\ddot{x}_g - \mu_k sign(\dot{x})\big(g + \ddot{y}_g\big) \tag{2}$$

Where $\ddot{x}$ and $\dot{x}$ are the horizontal acceleration and velocity of the center of mass of the rigid bock, $\ddot{y}_g$ and $\ddot{x}_g$ are the vertical and horizontal ground accelerations, μ_k is the coefficient of kinetic friction, and g is the acceleration due to gravity.

Rocking

A pure rocking response begins when the following condition is met, given that there is sufficient friction present to prevent sliding. The criteria for initiation into the rocking mode is provided by the following equation:

$$\big(g + \ddot{y}_g\big)\tan\alpha < \big|\ddot{x}_g\big| \tag{3}$$

2

where $\ddot{x}_g$ and $\ddot{y}_g$ are the horizontal and vertical ground acceleration, α is the critical angle of the rigid body (see Figure 1b), and g is the acceleration due to gravity. The equation of motion for a pure rocking response can be derived via Lagrangian dynamics resulting in the following:

$$\ddot{\theta} = \frac{mR}{mR^2 + I}\left[-sign(\theta)g\sin(\alpha - |\theta|) - \ddot{x}_g\cos(\alpha - |\theta|)\right] \tag{4}$$

In this equation, the rotational motion of the block is represented by $\ddot{\theta}$, the angular acceleration, and θ, the rotational displacement. The constants m, R, and I are the mass of the block, rocking radius, and moment of inertia, respectively (see Figure 1b). Note, the signum function and the absolute value of theta included in the horizontal and vertical terms are to account for both positive and negative angular rotation.

When a block is under pure rocking motion it pivots around one corner at a time then switches to the corresponding corner which causes an impact between the block and its foundation. This is modeled through a coefficient of restitution, or an instantaneous reduction of the angular velocity, $\dot{\theta}$:

$$\dot{\theta}_{n+1} = r\dot{\theta}_n \tag{5}$$

where $\dot{\theta}_{n+1}$ is the angular velocity of the block immediately after the impact, $\dot{\theta}_n$ is the angular velocity of the block just before the impact, and r is the coefficient of restitution, which is determined through conservation of angular momentum:

$$r = \left(1 - \frac{3}{2}\sin^2\alpha\right)^2 \tag{6}$$

where α is the critical angle of the block.

Slide-Rocking

Slide-rocking is a response mode characterized by simultaneous uplift and slip. This mode can be initiated from rest or initiated from either a sliding or rocking response. To initiate sliding during rocking, the absolute value of the ratio of the horizontal and vertical reaction forces on the block that prevents sliding must be greater than the coefficient of static friction [11]. First, the acceleration of the mass of the block in the horizontal and vertical directions, with respect to a rocking response, are needed. Static equilibrium equations are used to solve for the reaction forces for the x- and y-directions, R_x and R_y, yielding:

$$R_y = m(\ddot{y}_g + g) - sign(\theta)mR\ddot{\theta}\sin(\alpha - |\theta|) - mR\dot{\theta}^2\cos(\alpha - |\theta|) \tag{7}$$

$$R_x = m\ddot{x}_g - mR\ddot{\theta}\cos(\alpha - |\theta|) + sign(\theta)mR\dot{\theta}^2\sin(\alpha - |\theta|) \tag{8}$$

Where θ, $\dot{\theta}$, $\ddot{\theta}$ are the angular displacement, velocity, and acceleration of the block, m is the mass, R is the rocking radius, α is the critical angle, $\ddot{x}_g$ and $\ddot{y}_g$ are the horizontal components of the ground acceleration, and g is the acceleration due to gravity. Slide-rocking will initiate from a rocking response if the ratio of the reaction forces is greater than the coefficient of static friction:

$$\left|\frac{R_x}{R_y}\right| > \mu_s \tag{9}$$

where μ_s is the coefficient of static friction. In addition, slide-rocking can initiate from a sliding mode, where the conditions needed to initiate this come from a variation of Eq. (3). An inertial term, $m\ddot{x}$, is added to the inequality to account for the horizontal acceleration of the block during sliding [10]:

$$m(g + \ddot{y}_g)R\sin\alpha < m|\ddot{x} + \ddot{x}_g|R\cos\alpha \tag{10}$$

The equations of motion for slide-rocking can be similarly derived in a Lagrangian formulation, which yields a pair of equations for both angular acceleration ($\ddot{\theta}$) and horizontal acceleration ($\ddot{x}$) of the center of mass:

$$\ddot{\theta} = \frac{mR}{mR^2 + I}\left[-\cos(\alpha - |\theta|)\ddot{x} - sign(\theta)g\sin(\alpha - |\theta|) - \ddot{x}_g\cos(\alpha - |\theta|)\right] \tag{11}$$

$$\ddot{x} = -R\left[\cos(\alpha - |\theta|)\ddot{\theta} + sign(\theta)\sin(\alpha - |\theta|)\dot{\theta}^2\right] - \ddot{x}_g - \frac{F}{m} \tag{12}$$

where the variables are defined in accordance with Eq. (7) – Eq. (10) in addition to I, the moment of inertia and F, the work done by kinetic friction, which is defined as:

$$F = \mu_k sign(\dot{x})\left[m(g + \ddot{y}_g) - mR\dot{\theta}^2\cos(\alpha - |\theta|) + mR\ddot{\theta}\sin(\alpha - |\theta|)\right] \tag{13}$$

where each variable is similarly previously defined in addition to the coefficient of kinetic friction, μ_k. In this equation, the direction of the block's velocity, $\dot{x}$, determines the sign of the frictional force.

Since slide-rocking is a combination of two modes, the unique principles of rocking and sliding both apply (i.e. restitution). For example, a body still experiences restitution and may overturn if the angle of rotation is sufficiently large. For a pure rocking mode, restitution only affects the magnitude of the angular velocity (see Eq. (5)), but for a slide-rocking case, the horizontal velocity must also be reduced after an impact [12]:

$$\dot{x}_{n+1} = rH\dot{\theta}_n \tag{14}$$

where $\dot{x}_{n+1}$ is the horizontal velocity of the block after impact, r is the coefficient of restitution (Eq. (6)), $\dot{\theta}_n$ is the angular velocity of the block before impact, and H is the height of the block. The equations of motion for slide-rocking, under specific conditions, simplify to pure sliding or rocking responses. In this case, if the all the θ terms in Eq. (12) are set equal to zero, the equation reduces to the sliding response from Eq. (2). Similarly, if all $\ddot{x}$ terms are set to zero in Eq. (11), it simplifies to Eq. (4), which is the equation of motion for pure rocking. Therefore, if the slide-rocking response is triggered, it is possible for the rigid body to transition to pure rocking or pure sliding without the need to switch integration to a different equation of motion.

Representative Response due to Pulse Motion

The equations derived above were integrated into a comprehensive MATLAB program, which requires five inputs: ground acceleration ($\ddot{x}_g$ and $\ddot{y}_g$), static and kinetic friction coefficients (μ_s and μ_k), as well as the base length (B) and height (H) of the rigid block. Eq. (1) and Eq. (3) determine the initial mode of response. Then, depending if sliding or rocking is triggered, the corresponding equations of motions are integrated to find the dynamic response of the block. The equations of motion are integrated using a 4th-5th order Runge Kutta time stepping scheme. At every time step, the inequalities in Eq. (9) and Eq. (10) are checked to determine if the equation of motion for integration needs to reflect the slide-rocking motion. In addition, the computed angular displacement time history is checked at each time step to identify if an impact event has occurred by detecting a sign change of the angular displacement. At these instances, restitution is applied using Eq. (5) and Eq. (6) for pure rocking cases and using Eq. (5), Eq. (6), and Eq. (14) for slide rocking cases. After restitution is applied, the integration continues using the updated values of angular and horizontal velocity. The integration is truncated if overturning is identified or the motion has sufficiently decayed after the end of the ground acceleration. Sample results of the developed program are included in Figure 2 for pure sliding and pure rocking motions as well as in Figure 3 for a slide-rocking response. A sine wave pulse was used for the input ground motion with varying amplitudes and frequencies for blocks of varying geometry and friction to demonstrate each mode individually.

EARTHQUAKE PULSE GENERATION

Near-field ground motion pulses were generated as input for the intensity measure study using the analytical model from Mavroeidis and Papageorgiou [13]. Synthetic ground motions enable the study of how a rigid body, such as a PBR, would behave under a wide variety of earthquake magnitudes and rupture distances. The earthquake magnitudes ranged from 6.5 to 8.5 with rupture distances of 5, 10 and 15 kilometers. For each magnitude-rupture distance pair, 250 pulses were generated for a combined total of 3750 pulses. The analytical equation for the near-field pulse motion in terms of velocity is:

$$v(t) = A\frac{1}{2}\left[1 + \cos\left(\frac{2\pi f_p}{\gamma}(t - t_0)\right)\right]\cos[2\pi f_p(t - t_0) + v] \tag{15}$$

The variable t_0 represents a time shift calibration factor, as specified by Mavroeidis and Papageorgiou. For simplicity, the value given to t_0 ensures that the pulse starts at time $t = 0$. The above formula requires additional inputs including pulse frequency (f_p), number of half-cycles (γ), phase angle (v), time shift (t_0), and pulse amplitude (A), which are obtained through Latin Hypercube sampling using the statistics presented by Rupakhety et al. [14]. Rupakhety et al. assumed that the logarithms of f_p and the velocity amplitude of the pulse (V_p) are normally distributed, and found the mean for each value using Eq. (16) and Eq. (17):

$$\log\left(\frac{1}{f_p}\right) = -2.87 + 0.47M_w \tag{16}$$

$$\log(V_p) = -5.17 + 1.98M_w - 0.14M_w^2 - 0.10\log(R^2 + 0.562) \tag{17}$$

where M_w is the moment magnitude and R is the distance of the near-fault earthquake pulse being considered. Note that these equations utilize a maximum moment magnitude of 7, and the amplitude of the velocity pulse is a function solely of the distance for larger magnitudes [14]. The standard deviations for the logarithms of pulse frequency and velocity amplitude are 0.18 and 0.16, respectively. γ is assumed to follow a normal distribution with mean and standard deviation of 1.8 and 0.4 [14]. The phase

angle was selected arbitrarily from the range of $\pi/2$ to $\pi/2$ [15]. Once these parameters are found, the amplitude, A, can be calculated by rearranging the equation for pulse velocity by Mavroeidis and Papageorgiou:

$$A = 2V_p \left[\frac{1}{\left(1 + \cos\left(\frac{2\pi f_p}{\gamma}(t - t_0)\right)\right) \cos\left[2\pi f_p(t - t_0) + \nu\right]} \right] \tag{18}$$

(a)

(b)

(c)

(d)

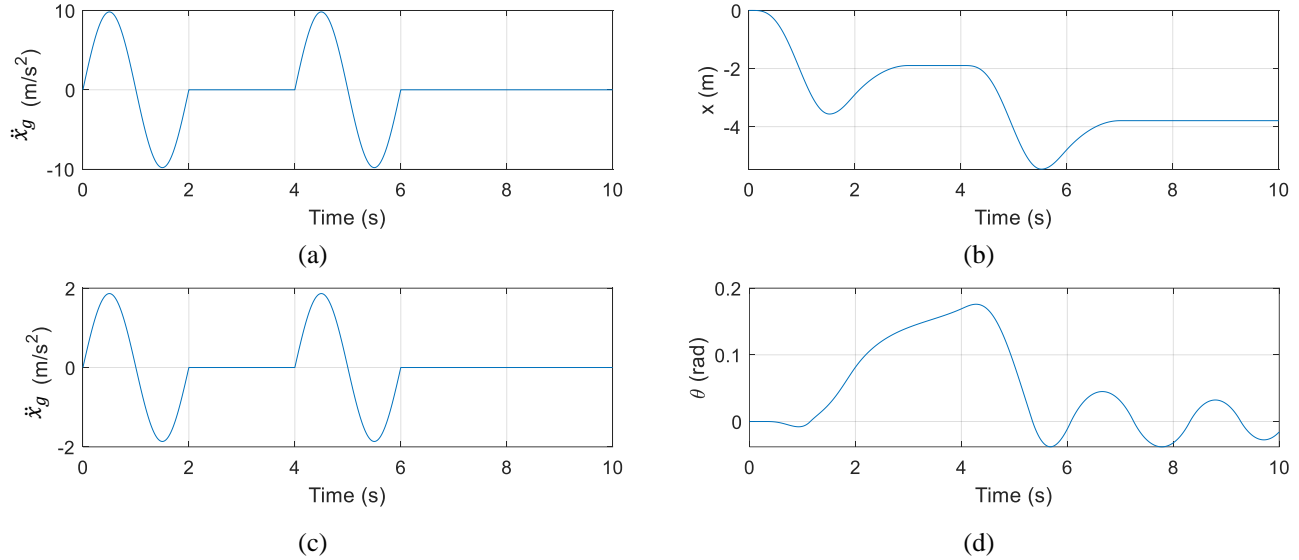*Figure 2. Pure sliding response of rigid block of R = 1.12 m, $\mu_s = 0.3$, and $\mu_k = 0.2$: (a) input base acceleration, and (b) displacement response. Pure rocking response of rigid block of R = 3.29 m, $\mu_s = 1.3$, and $\mu_k = 1.2$: (c) input base acceleration, and (d) angular displacement response.*
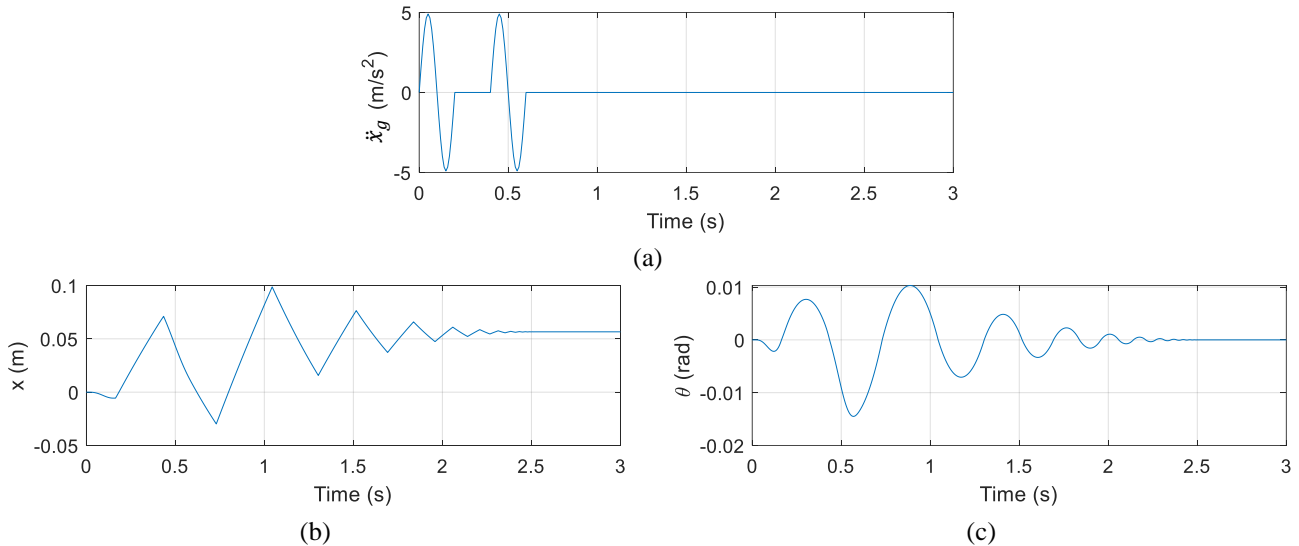

(a)

(b)

(c)

Figure 3. Slide-rocking response of rigid block of R = 2.06 m, $\mu_s = 0.3$, and $\mu_k = 0.2$: (a) input base acceleration, (b) displacement response, and (c) angular displacement response.

INTENSITY MEASURE STUDY

Earthquake intensity measures (IMs) are critical to relate seismic hazard to structural demand. In this case, the structural demand measures (DMs) used for precariously balanced rocks (PBRs) are the maximum absolute value horizontal and rotational displacements. When selecting IMs, it is important to consider efficiency and sufficiency. Efficiency of an IM refers to low variation in structural demand measures given an IM [16]. An IM is sufficient if it is independent of earthquake magnitude and

rupture distance [17]. Most PBR studies have utilized the peak horizontal or ground acceleration (PHA or PGA) or the peak ground acceleration normalized by the peak ground velocity (PGA/PGV) [2, 8, 9, 17, 18]. However, a comprehensive study of the efficiency of these measures has not been conducted. Therefore, this paper examines additional IMs to identify a more robust relationship between an IM and the multi-modal dynamic response of a PBR. The other IMs include: sustained maximum acceleration, effective design acceleration, predominant period, the ratio of maximum velocity to maximum acceleration, significant duration, RMS acceleration, characteristic intensity, Arias intensity, cumulative absolute velocity (CAV), response spectrum intensity (SI), velocity spectrum intensity (VSI), acceleration spectrum intensity (ASI), and effective peak velocity [19]. For the spectral intensity quantities, eight different period ranges were examined.

The IM study was conducted using a set of geometries targeting pure rocking and pure sliding subject to 3750 synthetic earthquake pulses. The pure sliding case used a block with a critical angle, α, of 45° and friction coefficients of 0.1 for both static and kinetic. Conversely, the critical angle of the rocking case block was much lower, $α = 11.31°$ and the static and kinetic friction coefficients were 1.5 and 1.0, respectively. Next, a total of 37 ground motion IMs were calculated for each of the 3750 motions. Results were excluded from the regression analysis if excessive angular or horizontal displacement was observed to focus the study on realistic structural responses. Then, a linear regression analysis was conducted between the ground motion IMs and the maximum absolute value structural demands of the block. The regression was done on the dataset as a whole and for a sample of five magnitude-distance (M_w-R) pairs.

Sliding

The IMs that demonstrated the most robust probabilistic relationship with horizontal displacement due to sliding were SI, ASI, and CAV. The R^2 values for the overall dataset and five magnitude-distances pairs are presented in Table 1. Statistical values for PHV and PHA are also listed since these metrics have historically been used as IMs for structures undergoing rocking behavior [9, 17, 18]. Spectral intensity quantities in the intermediate period range and CAV displayed the most significant R^2 for a pure sliding response whereas both PHV and PHA had the least significant. SI, ASI, and CAV were calculated using Eq. (19), (20), and (21) with a critical damping ratio of 5% [19]:

$$SI = \int_{T_1}^{T_2} PSV(\zeta, T)dT \tag{19}$$

$$ASI = \int_{T_1}^{T_2} S_a(\zeta, T)dT \tag{20}$$

$$CAV = \int_{0}^{T_d} |a(t)|dt \tag{21}$$

where PSV is the pseudo-spectral velocity, ζ is the damping ratio, T is the period, T_1 and T_2 are the integration limits for period, S_a is the spectral acceleration, $a(t)$ is the ground acceleration, t is time, and T_d is the total duration of the ground acceleration time history. From Table 1, the relationship between the IM and DM vary noticeably between individual magnitude-distance pairs. For example, the earthquake pulses with magnitudes of 7 and 8 at a rupture distance of 10 km had the highest R^2 statistics. Magnitude 7 records exhibit the most significant R^2 values when PHV and PHA are excluded. CAV appears to be the most sufficient IM since it has the least variation in R^2 across the five magnitude-rupture distance pairs. The other parameter produced through the linear regression analyses was the slope of the regression line. The scatter plots for the five most significant IMs are shown in Figure 4. The blue markers represent pure sliding response while the orange markers indicate a record that produced no response from the block. The green line is the best-fit line for the data. Substantial scatter can be seen in the plots from Figure 4, indicating that the IMs are not very efficient and hinting that additional intensity measures may be required to adequately predict the sliding response.

Rocking

Similar to pure sliding, ASI and SI for intermediate period ranges had the highest correlation with rotational displacement due to rocking. The spectral intensity quantities demonstrated much more significant R^2 statistics than PHV and PHA with values of 0.5266 for ASI (1.0 – 2.5 s) compared to 0.1789 for PHV and 0.2403 for PHA, despite these two IMs being the most-used for rocking structures (Table 2). This trend can be seen in the overall dataset as well as in the individual magnitude-distance pairs. It is noted that the pulses with a magnitude of 8.5 and rupture distance of 10 km showed the highest R^2 among the top five IMs. This makes sense given that very intense motions are needed to initiate and sustain rocking motions. The variety of R^2 values between the magnitude-distance pairs may be indicative of insufficiency for ASI, SI, PHV, and PHA. In Figure 5 below, the blue markers signify a pure rocking response, the orange markers show records that did not generate a rocking response, and the yellow marker depicts the overturning cases. Again, the green line is the best-fit line produced through linear regression analysis. These scatter plots show less variability in the maximum absolute value rotational displacement, which

indicates the efficiency of the IMs. While not directly presented in this paper, additional cases focused on slide-rocking response were analyzed as part of this study. Similar intensity measures emerged as optimal – namely, the spectral intensities over the intermediate range. The R^2 statistics, in these cases, were on par with those reported for both sliding and rocking and even exceeded them for a number of slide-rocking blocks.

Table 1. R^2 values for IMs and sliding response for the overall dataset and individual magnitude-distance pairs.

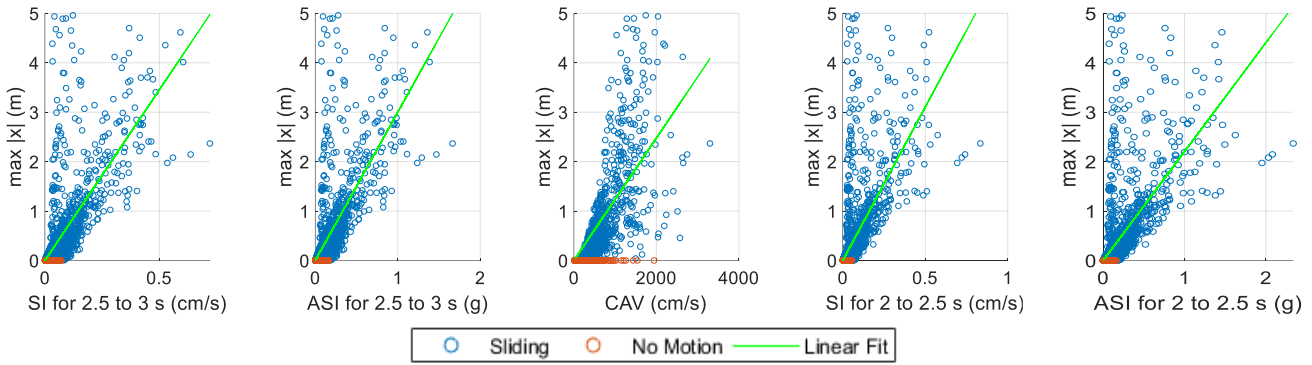| Intensity Measure	R^2					Overall R^2
	M6.5 R10	**M7 R10**	**M7.5 R10**	**M8 R10**	**M8.5 R10**	
SI (2.5 to 3.0 s)	0.4096	0.6139	0.4995	0.5128	0.4610	0.4992
ASI (2.5 to 3.0 s)	0.4070	0.6127	0.4955	0.5127	0.4581	0.4967
CAV	0.4289	0.4872	0.4644	0.5675	0.4645	0.4712
SI (2.0 to 2.5 s)	0.3573	0.5449	0.3663	0.5257	0.3773	0.4069
ASI (2.0 to 2.5 s)	0.3557	0.5431	0.3626	0.5245	0.3743	0.4040
PHV	0.1465	0.1109	0.1071	0.2839	0.1123	0.1461
PHA	0.2370	0.1609	0.1910	0.2608	0.1721	0.1754

Figure 4. Horizontal displacement due to sliding vs. intensity measures for all M-R pairs.

Table 2. R^2 values for IMs and rocking response for the overall dataset and individual magnitude-distance pairs.

| Intensity Measure	R^2 value per Magnitude-Distance Pair					Overall R^2
	M6.5 R10	**M7 R10**	**M7.5 R10**	**M8 R10**	**M8.5 R10**	
ASI (1.0 to 2.5 s)	0.6807	0.5515	0.4981	0.5860	0.7455	0.5266
SI (1.0 to 2.5 s)	0.6794	0.5572	0.5030	0.5452	0.7738	0.5201
SI (1.0 to 1.5 s)	0.6075	0.5317	0.4464	0.6855	0.5829	0.5104
ASI (1.0 to 1.5 s)	0.6008	0.5308	0.4402	0.6918	0.5718	0.5080
ASI (1.5 to 2.0 s)	0.6641	0.5246	0.4947	0.5447	0.7875	0.5031
PHV	0.1688	0.1483	0.1156	0.4273	0.2121	0.1789
PHA	0.3085	0.2559	0.2462	0.1766	0.2545	0.2403
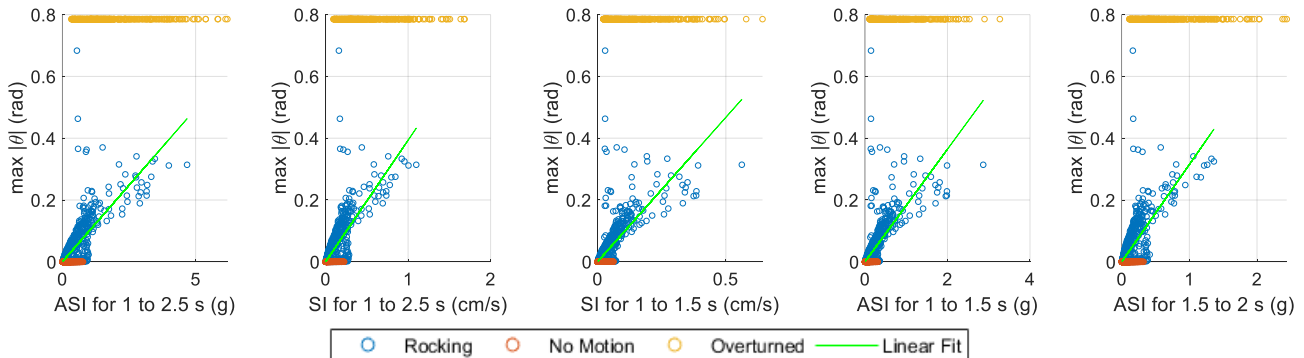
Figure 5. Rotational displacement due to rocking vs. intensity measures for all M-R pairs.

CONCLUSIONS

The equations of motion for a two-dimensional rigid body subject to seismic excitations were presented for sliding, rocking and slide-rocking modes. Previous authors have mainly studied the rocking responses of precariously balanced rocks excluding sliding from their models, whereas this study included an analysis of sliding response. Several thousand synthetic earthquake pulses were produced and used as input to a set of two-dimensional freestanding structures in an intensity measure study for rocking, sliding, and slide-rocking cases. The data produced in this study suggests that traditional intensity measures (IMs) used for rocking blocks, like peak horizontal velocity or acceleration, are not the most sufficient or efficient IMs. IMs that measure spectral quantities in the intermediate period range showed stronger correlations with all modes, including sliding, rocking, and slide-rocking demands. However, significant scatter was observed for even the best performing IMs. Therefore, this study should be further expanded to include vector-valued IMs.

ACKNOWLEDGMENTS

REFERENCES

[1] Brune, J. N. (1996). Precariously balanced rocks and ground-motion maps for southern California. *Bulletin of the Seismological Society of America*, *86*(1A), 43-54.

[2] Baker, J. W., Abrahamson, N. A., Whitney, J. W., Board, M. P., & Hanks, T. C. (2013). Use of fragile geologic structures as indicators of unexceeded ground motions and direct constraints on probabilistic seismic hazard analysis. *Bulletin of the Seismological Society of America*, *103*(3), 1898-1911.

[3] Anderson, J. G., Biasi, G. P., & Brune, J. N. (2014). Precarious rocks: Providing upper limits on past ground shaking from earthquakes. In Earthquake Hazard, Risk and Disasters (pp. 377-403).

[4] Bell, J. W., Brune, J. N., Liu, T., Zreda, M., & Yount, J. C. (1998). Dating precariously balanced rocks in seismically active parts of California and Nevada. *Geology*, *26*(6), 495-498.

[5] Balco, G., Purvance, M. D., & Rood, D. H. (2011). Exposure dating of precariously balanced rocks. *Quaternary Geochronology*, *6*(3-4), 295-303.

[6] Housner, G. W. (1963). The behavior of inverted pendulum structures during earthquakes. *Bulletin of the seismological society of America*, *53*(2), 403-417.

[7] Shi, B., Anooshehpoor, A., Zeng, Y., & Brune, J. N. (1996). Rocking and overturning of precariously balanced rocks by earthquakes. *Bulletin of the Seismological Society of America*, *86*(5), 1364-1371.

[8] Anooshehpoor, A., Brune, J. N., & Zeng, Y. (2004). Methodology for obtaining constraints on ground motion from precariously balanced rocks. *Bulletin of the Seismological Society of America*, *94*(1), 285-303.

[9] Purvance, M. D., Anooshehpoor, A., & Brune, J. N. (2008). Freestanding block overturning fragilities: Numerical simulation and experimental validation. *Earthquake Engineering & Structural Dynamics*, *37*(5), 791-808.

[10] Taniguchi, T. (2002). Non-linear response analyses of rectangular rigid bodies subjected to horizontal and vertical ground motion. *Earthquake engineering & structural dynamics*, *31*(8), 1481-1500.

[11] Taniguchi, T. (2004). Experimental and analytical study of free lift-off motion induced slip behavior of rectangular rigid bodies. *Journal of pressure vessel technology*, *126*(1), 53-58.

[12] Shenton III, H. W., & Jones, N. P. (1991). Base excitation of rigid bodies. I: Formulation. *Journal of Engineering Mechanics*, *117*(10), 2286-2306.

[13] Mavroeidis, G. P., & Papageorgiou, A. S. (2003). A mathematical representation of near-fault ground motions. *Bulletin of the seismological society of America*, *93*(3), 1099-1131.

[14] Psycharis, I. N., Fragiadakis, M., & Stefanou, I. (2013). Seismic reliability assessment of classical columns subjected to near-fault ground motions. *Earthquake engineering & structural dynamics*, *42*(14), 2061-2079.

[15] Rupakhety, R., Sigurdsson, S. U., Papageorgiou, A. S., & Sigbjörnsson, R. (2011). Quantification of ground-motion parameters and response spectra in the near-fault region. *Bulletin of Earthquake Engineering*, *9*(4), 893-930.

[16] Luco, N., & Cornell, C. A. (2007). Structure-specific scalar intensity measures for near-source and ordinary earthquake ground motions. *Earthquake Spectra*, *23*(2), 357-392.

[17] Padgett, J. E., Nielson, B. G., & DesRoches, R. (2008). Selection of optimal intensity measures in probabilistic seismic demand models of highway bridge portfolios. *Earthquake Engineering & Structural Dynamics*, *37*(5), 711-725.

[18] Dimitrakopoulos, E. G., & Paraskeva, T. S. (2015). Dimensionless fragility curves for rocking response to near-fault excitations. *Earthquake Engineering & Structural Dynamics*, *44*(12), 2015-2033.

[19] Kramer, S.L., 1996, Geotechnical Earthquake Engineering: Prentice-Hall, Inc., 273.